


Microphysiological system to address the opioid crisis: A novel multi-organ model of acute opioid overdose and recovery

Aakash Patel^a, Suruchi Poddar^a, Daniel Nierenberg^a, Stephanie Lang^a, Hao Wang^a, Camilly Pestana Pires DeMello^a, Julio Gamarra^a, Alisha Colon^a, Paula Kennedy^b, Jeffry Roles^b, Jules Klion^b, Will Bogen^b, Christopher Long^b, Xiufang Guo^a, Patrick Tighe^c, Stephan Schmidt^c, Michael L. Shuler^b, James J. Hickman^{a,b,*} 

^a University of Central Florida, NanoScience Technology Center, 12424 Research Parkway, Suite 400, Orlando, FL 23826, United States

^b Hesperos, Inc, 12501 Research Parkway, Suite 100, Orlando, FL 32826, United States

^c Department of Pharmaceutics, College of Pharmacy, Center for Pharmacometrics and Systems Pharmacology, University of Florida, Orlando, Florida, 32610 USA

ARTICLE INFO

Keywords:

Microphysiological systems
Opioid overdose
Multi-organ
Body-on-a-chip
Off-target toxicity
Drug development

ABSTRACT

Opioids have been the primary method used to manage pain for hundreds of years, however the increasing prescription rate of these drugs in the modern world has led to a public health crisis of overdose related deaths. Naloxone is the current standard treatment for opioid overdose rescue, but it has not been fully investigated for potential off-target toxicity effects. The current methods for pharmaceutical development do not correlate well with pre-clinical animal studies compared to clinical results, creating a need for improved methods for therapeutic evaluation. Microphysiological systems (MPS) are a rapidly growing field, and the FDA has accepted this area of research to address this concern, offering a promising alternative to traditional animal models. This study establishes a novel multi-organ MPS model of acute opioid overdose and rescue to investigate the efficacy and off-target toxicity of naloxone in combination with opioids. By integrating primary human and human induced pluripotent stem cell (hiPSC)-derived cells, including preBöttinger complex neurons, liver, cardiac, and skeletal muscle components, this study establishes a novel functional multi-organ MPS model of acute opioid overdose and rescue to investigate the efficacy and off-target toxicity of naloxone in combination with opioids, with clinically relevant functional readouts of organ function. The system was able to successfully exhibit opioid overdose using methadone, as well as rescue using naloxone evidenced by the neuronal component activity. In addition to efficacy, the multi-organ platform was able to characterize potential off-target toxicity effects of naloxone, specifically in the cardiac component.

Introduction

The use of opioids as a medical tool to combat chronic pain has been in practice since before the 1600s and became the standard treatment for both chronic and acute pain throughout the 19th century. Over the years, multiple opiates have been developed and released to the public for the purpose of pain management, with morphine being one of the first industrially produced forms in the 1820s, followed by heroin in 1898. Hand in hand with the increasing use of opioids, opioid abuse also continued to grow, as many of the initial opiate medications, such as heroin, were available over the counter leading to self-medication. While heroin was eventually banned and classified as a Schedule 1

substance, other opioids continued to be developed, and heavily used throughout the years (Dasgupta, 2020). Opioid overdose was officially declared to be a public health crisis in the United States in 2017, in response to a growing number of opioid overdose related deaths (Chhatwal et al., 2023). In 2016, more than 64,000 people died from opioid overdoses, with that number growing to over 91,000 in 2020 according to the Center for Disease Control. The rise in opioid overdose related death is due to 3 specific stages: 1) the introduction of new opioids, notably OxyContin, which because of its sustained release method of action was claimed to be non-addictive, leading to an increase in prescription rates, 2) an increase in heroin addiction, mainly in patients who were originally prescribed clinical painkillers, and 3) the

* Corresponding author.

E-mail address: jhickman@ucf.edu (J.J. Hickman).

<https://doi.org/10.1016/j.crttox.2024.100209>

Received 10 May 2024; Received in revised form 2 December 2024; Accepted 10 December 2024

Available online 18 December 2024

2666-027X/© 2024 The Authors. Published by Elsevier B.V. This is an open access article under the CC BY-NC-ND license (<http://creativecommons.org/licenses/by-nc-nd/4.0/>).

introduction of novel synthetic opioids, of which the most popular is fentanyl (Robert et al., 2023). As a result, opioid overdose has become the leading cause of accidental death in the country, and methods to prevent and treat opioid overdose have become a critical area of research, especially after the COVID-19 pandemic (Friedman and Gjersing, 2023). Opiates are classified into three main categories: natural, such as morphine and codeine, semisynthetic which include drugs such as oxycodone, naloxone, and oxymorphone, and synthetic such as methadone and fentanyl. Semisynthetic opioids are structurally similar to morphine, while synthetics do not share structural similarities with morphine but pharmacologically have the same targets (Dasgupta, 2020). All three types of opioids act on the body through interaction with mu, delta, and kappa opioid receptors, which are found on multiple cell types throughout the body (Barron, 1999; Bateman et al., 2023; Boyella et al., 2008; Evans and Smith, 2004; Zare et al., 2023; Dasgupta, 2020).

Currently, the most common treatment for opioid overdose is the drug naloxone, also known as Narcan, first developed by Jack Fishman in the 1960's. While originally developed as a compound to alleviate some of the non-lethal side effects of chronic opioid use, in 1971 it was approved by the FDA as a treatment for reversing opioid overdose (Campbell, 2019). Acting as an opioid antagonist, naloxone competitively binds opioid receptors, primarily the μ -opioid receptor, displacing opioid agonists from these receptors and reversing OIRD (Robinson and Wermeling, 2014). While this drug has been thought to be relatively safe and effective as a treatment to reverse opioid overdose, naloxone's off-target toxicity has not been fully investigated.

Microphysiological systems (MPS) are a rapidly growing area of research that can be used to evaluate the efficacy of therapeutic treatments as well as identify potential off target toxicity risks (McAleer et al., 2019). Currently, animal based pre-clinical trials are the most widely utilized method for screening compounds before reaching the clinical trial stage. While potential therapeutics may show success in pre-clinical trials, 89 % of novel drugs fail once reaching clinical trials, highlighting the often poor translatability of animal models to humans (Cook et al., 2014). This attrition rate leads to the loss of millions of dollars and thousands of hours spent on the evaluation of new therapeutics, contributing to an overall decrease in the efficiency of the drug development process, creating a need for improved pre-clinical investigation strategies (Hughes, 2008; Cook et al., 2014). Multi-organ platforms utilizing more than one human or animal cell-based models of organs can provide functional, as well as biomarker data, that can accurately recapitulate and predict the response of human organs in response to chemicals or potential therapeutics. Most current in vitro platforms consist of cells cultured in a multiwell platform which are then dosed with a potential therapeutic. These types of in vitro platforms lack physiological relevance due to the isolation of the cells, lack of exchange of metabolites between different organ types, no physiological flow of a common blood surrogate medium, and the absence of mechanical forces associated with fluid dynamics present in the body. Multi-organ platforms present the advantage of having multiple organs interconnected on the same platform, allowing metabolite exchange between organs in a common medium (Miller and Shuler, 2016). With the recent passage of the FDA Modernization Act 2.0, the United States Congress has recognized their value, and specified the use of such in vitro models as viable replacements for animal models in preclinical trials, with the hope of increasing the efficiency of the drug screening process (Modernization Act, 2023).

Through the use of a multi-organ platform, we aimed to create a functional model of opioid overdose utilizing a combination of primary human and human induced pluripotent stem cell (hiPSC)-derived cells to study the efficacy and off-target toxicity of naloxone. Methadone was used to induce opioid overdose in order to confirm the efficacy of naloxone as a reversal agent. Methadone was chosen for this study as it is a well-studied synthetic opioid, which is the primary opioid utilized to treat substance abuse. The MPS platform consists of preBötzing

complex neurons (hiPSC-derived), hepatic (primary), cardiac (hiPSC-derived) (Guo et al., 2024), and skeletal muscle (hiPSC-derived) components. Functional readouts were performed using microelectrode arrays (MEAs) to measure neuronal action potential and cardiac conduction velocity as well as cardiac minimal inter-spike interval (mISI) a correlate of QT interval, cantilevers (CLs) to measure contractile amplitude and beat frequency of cardiomyocytes, and skeletal muscle contractile amplitude, with liver metabolism measured via a CYP assay. The preBötzing complex (preBötC) is the region of the brainstem composed of both excitatory and inhibitory neurons, which are responsible for the regulation of inspiratory rhythm generation, considered to be the most critical circuit regulating respiration. This complex, via other downstream follower neurons, activate upper airway respiratory muscles such as the diaphragm (Bateman et al., 2023; Guo et al., 2024). Excess binding of opiates to these opioid receptor expressing neurons can cause opioid induced respiratory depression (OIRD), slowing down or stopping breathing, resulting in death via asphyxiation making these neurons a crucial component in any in vitro model of opioid overdose (Guo et al., 2024). The preBötzing complex (preBötC) component establishes the occurrence of an opioid overdose event, and subsequent rescue with naloxone, while the other organ components were used to determine any off-target toxicity that may occur in the other organs. Through this research, a better understanding of the off-target toxicity of naloxone in combination with the effects of opioid overdose on the different organs was established. This specific study serves as a proof of concept, showcasing the ability of this platform to potentially improve the treatment of opioid overdose by providing a clinically relevant platform to test other newly developed treatments for opioid overdose, as well as different opioids. Considering the broader context of MPS systems as an emerging field of research, this study can also serve as a valuable contribution in the validation of the applicability of this type of pre-clinical approach. By demonstrating the similarities between data collected from an in vitro system such as this with previous in vivo knowledge, the field of MPS systems as a whole can be advanced.

Methods and Materials

Cantilever fabrication and surface modification

Cantilever microelectromechanical systems were prepared as described previously (Stancesu et al. 2015). Cantilever chips consisted of 2 rows of 16 cantilevers, 4 μm thick, 150 μm wide for cardiac cantilevers, 100 μm wide for skeletal muscle cantilevers, and 737 μm long, fabricated from silicon-on-insulator wafers with a 4 μm device layer with 1 μm buried oxide. The cantilevers were created in the device layer, and a window for each of the 2 rows was produced under the cantilevers using standard photolithographic patterning and deep reactive ion etching. Cantilevers for iPSC-derived skeletal muscle plating were first plasma treated (Harrick Plasma), then coated with 2-[methoxypoly(ethyleneoxy)propyl]trimethoxysilane (PEG) in toluene to create a cytophobic substrate, after which 50 μm lines were created on the individual cantilevers via UV laser ablation, utilizing a 193 nm ArF excimer laser (Lambda Physik, Santa Clara, CA) through a quartz photomask. Following laser ablation, surfaces were backfilled with 3-(trimethoxysilyl)propyl diethylenetriamine silane (DETA) in toluene to provide a triamine substrate to promote protein and cell attachment. After surface modification, cantilevers were sterilized in 70 % IPA, and coated with Collagen 1 for 2 h at room temperature before iPSC-derived myoblast seeding. Cantilevers for iPSC-derived cardiomyocytes (Cellular Dynamics Inc.) were manufactured in the same method, with the difference of the cantilever width being 150 μm instead of 100 μm . Cantilevers for cardiomyocytes were plasma cleaned, sterilized, and coated with fibronectin for 30 min at 37 °C before cell seeding.

Microelectrode array fabrication and surface modification

Custom microelectrode arrays (MEAs) were fabricated, modified, and characterized as described in Oleaga et al (Oleaga et al., 2019). Briefly, the fabrication process consisted of electron beam evaporation of 10 nm titanium and 50 nm platinum to create wires and electrodes onto a fused silica substrate. Ten electrodes of 200 μm diameter, and a single 2000 μm diameter ground electrode were laid down, with the wires insulated with a three 150 nm layers of silicon oxide, silicon nitride, and silicon oxide via plasma enhanced chemical vapor deposition, and etched using reactive ion etching with gas mixtures of CHF₃ and O₂. MEAs for cardiomyocyte plating were modified with PEG, a u-pattern was ablated across the 10 electrodes and coated with fibronectin as described for cardiac cantilevers. MEAs for preBöttinger neurons were coated with PEG, a neuronal pattern was ablated, and backfilled with DETA. These MEAs were then coated with a mixture of laminin (Fisher Scientific) and fibronectin (Millipore Sigma) overnight at 4 °C, followed by 2-hour incubation at 37 °C, immediately prior to cell seeding.

Cell Culture

Hepatocyte plating

Primary human hepatocytes were purchased from Novabios (NHPHepatocytes) and plated onto rat tail Collagen 1 (Gibco) coated 15 mm round glass coverslips 7 days prior to multi-organ system assembly. First, 15 mm round coverslips were plasma treated and sterilized in 70 % IPA. After drying, Collagen 1 was added to the coverslips in a bubble, and incubated at 37 °C for 30 min. Hepatocytes were thawed in a water bath and transferred into thaw medium (Novabios, NHTM-P). Cells in thaw buffer were centrifuged for 10 min at 100g with soft acceleration and brake. Supernatant was aspirated, cells were resuspended in 4 mL of hepatocyte plating medium (Novabios, NHPM), and a cell count was performed. Based on the cell count, additional plating medium was added to the cell suspension to bring the concentration of the cell solution to 2,500,000 cells/mL. Collagen 1 was aspirated from coverslips, and hepatocytes in plating medium were added to Collagen 1 coated coverslips in a 100 μL bubble to achieve a plating density of 250,000 cells per coverslip. Hepatocytes were then allowed to adhere to coverslips for 2 h at 37 °C, after which the medium was refreshed with 100 μL of plating medium. Following an additional 2 h incubation, plating medium was removed, and the wells were filled with 1 mL of hepatocyte maintenance medium (Novabios, NHMM). The following day, a full medium exchange with maintenance medium was performed to remove non-adherent cells. One day prior to multi-organ system assembly, a collagen hydrogel was added to hepatocyte coverslips by transferring coverslips to a new, dry, well plate, and applying 90 μL bubble of hydrogel mix containing 1x DPBS, 1 N NaOH, and rat tail Collagen 1 (Gibco). Hydrogel coated coverslips were incubated at 37 °C for 1 h, then replenished with 1 mL of maintenance medium. Cells were maintained in hepatocyte maintenance medium until assembly into multi-organ systems.

Cardiomyocyte plating

iPSC-derived cardiomyocytes were purchased from Cellular Dynamics Inc. (CDI, CMC-100-0010-001). Cantilevers for cardiac plating were prepared by plasma cleaning, sterilization in 70 % IPA, and placing on top of 22 mm 1,1,2,2-perfluorooctyl trichlorosilane (13F) coated coverslips. MEAs were prepared as described above, with PEG ablated cardiac U-patterning, and sterilized in 70 % IPA. After surfaces were dry, polydimethylsiloxane (PDMS) barriers were attached to MEAs to restrict plating area to the electrodes, and onto cantilevers to restrict plating area to cantilevers. 200 μL of fibronectin (Millipore Sigma) at a concentration of 50 $\mu\text{g}/\text{mL}$, and 100 μL of fibronectin at a concentration of 10 $\mu\text{g}/\text{mL}$ were added to cantilevers and MEAs respectively. Surfaces were then incubated at 37 °C for 30 min, followed by rinsing with 1x

PBS, twice for cantilevers, and once for MEAs. Cells were then thawed in a 37 °C water bath, and transferred to 50 mL conical, followed by drop-by-drop addition of 9 mL of plating medium (CDI, CMM-100-110-005). Cells were centrifuged at 250g for 5 min with soft brake and acceleration. Supernatant was aspirated, and cells were resuspended in 1 mL of fresh plating medium, and counted. Cells were then split into two tubes, one tube with a cell concentration of 200,000 cells/200 μL of plating medium, and the second tube with a cell concentration of 50,000 cells/100 μL of plating medium for cantilevers, and MEAs respectively. 200 μL of the first cell solution was added to the cantilevers, and 100 μL of the second cell solution was added to the MEAs, followed by incubation of both surfaces at 37 °C for 2 h. Following incubation, cantilevers and MEAs were topped off with an additional 300 μL of a 50:50 mix of plating medium:cardiac maintenance medium. The next day, 1.5 mL of cardiac maintenance medium consisting of 5x B27, 1x AB/AM, 10 mM HEPES, 1x MEM/NEAA, 1x Glutamax, 0.5 $\mu\text{g}/\text{mL}$ hydrocortisone, 0.1 $\mu\text{g}/\text{mL}$ L-tyrosine, 10 ng/mL EGF, and 0.2 M dextrose, in Ultraculture Medium (Bio Whittaker Cambrex) was added to each surface. 2–3 days following this, cantilevers were removed from 13F coverslips, and a full medium exchange was performed with 2 mL of cardiac maintenance medium.

iPSC-derived skeletal muscle plating (SKM)

iPSC-derived myoblasts were differentiated from ND41865 wildtype iPSCs (Coriell), following the protocol from Guo et al. (Guo et al., 2020). Myoblasts were passaged and frozen down at P5 for use in multi-organ experiments. Myoblasts were thawed 7 days prior to multi-organ system assembly following the protocol stated in Guo et al., with the exception of using Lonza SKGM (Lonza, Basel, Switzerland), instead of the mentioned MyoCult medium for initial plating. PEG/DETA modified cantilevers were sterilized in 70 % IPA, placed on 22 mm 13F coverslips after drying, and polydimethylsiloxane (PDMS) barriers were attached to restrict plating area to cantilevers. Cantilevers were then coated with rat tail Collagen 1 (Gibco), at RT for 2 h. Following collagen coating, cantilevers were rinsed with 1x PBS three times, and myoblasts were plated onto cantilevers at a seeding density of 100 cells/ mm^2 . Once myoblasts were confluent, they were switched from Lonza to DKHI medium. After 2 days in DKHI, cultures were switched to and maintained in NbA4 (Brainbits) until assembly into multi-organ systems.

iPSC-derived PreBöttinger complex neuron (PreBötC) plating

iPSC-derived PreBöttinger complex (preBötC) neurons were differentiated from ND41865 wildtype iPSCs (Coriell), following the protocol from Guo et al. (Guo et al., 2024). Prior to plating, PEG/DETA modified MEAs were sterilized in 70 % IPA, polydimethylsiloxane (PDMS) barriers were attached to MEAs to restrict plating area to the electrodes, and coated with laminin + fibronectin, as mentioned above. Following protein coating, MEAs were rinsed once with 1x PBS, and preBötC neurons were thawed and plated 7 days prior to multi-organ system assembly. PreBötC neurons were thawed in a 37 °C water bath, added directly into 9 mL of preBöttinger neuron medium (PBNM) (formulation found in Guo et al.), and centrifuged at 260g for 5 min. Following centrifugation, the supernatant was aspirated, and cells were resuspended in 1 mL of fresh PBNM. A cell count was performed, and cells were seeded onto MEAs at a density of 600 cells/ mm^2 . Cells were maintained in PBNM until assembly into multi-organ systems.

Multi-organ system housing fabrication

The multi-organ system itself consists of two poly(methyl methacrylate) pieces, a top and a bottom, and three PDMS gaskets, a top, bottom, and middle piece, to define the medium flow path, and compartments for the individual bio-MEMs devices. Holes for feeding reservoirs, slots for stimulation electrodes for cantilevers, and slots for zebra connectors to make contact with the electrode pads of the MEAs were made by laser cutting. A more detailed housing fabrication process

can be found in [Oleaga et al., 2016](#).

Immunocytochemistry

Before any multi-organ experiments were performed, individual cell types were immunostained for μ -, δ -, κ - opioid receptors, and TLR4. Cells were fixed at Day 7 with freshly prepared 4 % paraformaldehyde in PBS for 15 min and then rinsed twice with PBS (pH 7.2, without Mg^{2+} and Ca^{2+}). Next, they were permeabilized with a 0.1 % Triton X-100/PBS solution for 15 min at room temperature. Nonspecific binding sites were blocked with the permeabilization solution and a blocking buffer (5 % donkey serum + 0.5 % BSA in PBS) for 1 h at room temperature. Cells were incubated with primary antibodies in blocking buffer at 4 °C overnight, using the following primary antibodies: OPRD1 for δ -opioid receptors (Novus, NLS222), OPRM1 for μ -opioid receptors (Novus, NB100-1620), KOR-1 for κ -opioid receptors (Santa Cruz Biotechnology, sc-374479), and anti-TLR4 for toll-like receptor 4 (Novus, NB100-56566). The next day, the primary antibody/blocking buffer solution was removed, and the cells were rinsed 3 \times with PBS. Then, AlexaFluor 488 and 568 antibodies were diluted 1:250 in blocking buffer and incubated at room temperature for 2 h in the dark. The secondary antibody/blocking buffer solution was removed, and cells were rinsed 3 \times with PBS and then incubated for 5 min in a 1:1000 DAPI in PBS solution. After 5 min, the DAPI/PBS solution was removed, and the cells were rinsed 3 times with PBS, before being mounted onto glass slides using a VectaShield mounting medium (Invitrogen P36931). Primary antibody specificity was validated by performing secondary only controls, where the same staining process was performed with the exception of no primary antibody being added. Mounted samples were imaged with an Axioskop 2 mot plus upright spinning disk confocal microscope (Carl Zeiss). Imaging parameters were determined using the secondary controls to ensure exclusion of false positive signal. Staining was performed for 3 independent times.

Multi-organ system assembly

Three days before assembly, all the multi-organ system housing components were put through a three-step preparation process. 1) acrylic housings and PDMS gaskets were sonicated three times in diH_2O , and placed in a laminar flow hood to dry, 2) housing acrylic and PDMS gaskets were sterilized by dipping into a tub of 70 % IPA, gaskets placed and aligned onto housings while still wet with IPA, then laid out to dry in laminar flow hood for a minimum of 4 h, 3) the night before assembly, 3 % bovine serum albumin (BSA) in 1x PBS was laid onto the housings (3 mL on bottom housings, 2 mL on top housing) in the flow paths to confer hydrophilic properties to the flow area, and the compartments where the bio-MEMs devices would be placed, and left overnight. The next day, immediately prior to system assembly, the BSA solution was aspirated and replaced with 2 mL of multi-organ system medium (MOSM) (formulation can be found in McAleer et al.) with osmolarity adjusted to 300 mOsm on the bottom housing ([McAleer et al., 2019](#)). Bio-MEMs devices were placed into their respective compartments, and the top housing was carefully placed onto the bottom housing and secured with 16 galvanized steel screws. Following assembly, systems were placed onto rockers in 37 °C, 5 % CO_2 incubators set to a tilt profile of 1° per minute. Systems were maintained in these incubator/rocker conditions with daily feedings of 600 μ L of 260 mOsm MOSM. Systems were maintained for 6 days before any functional testing was performed.

Functional testing

Cantilever measurements

A cantilever deflection system was used to measure the contractile force or amplitude of both cardiomyocytes and skeletal muscle, as previously described ([Pirozzi et al., 2013](#); [Stancescu et al., 2015](#)). A laser (Thorlabs) was directed at the ends of the cantilevers, from where it was

deflected onto a 2D Lateral Effect Position Sensor (Thorlabs). Contraction of the cells on the cantilevers caused the cantilever to bend, thereby shifting the position of the deflected laser on the detector. An automated directed peak detection program written in Python 2.7, measured the deflection of the laser to determine the average maximum amplitude of the resulting peaks, as well as contraction frequency. A modified version of Stoney's equation was then used to determine the force or amplitude of the contraction, based on the voltage output from the laser detector ([Pirozzi et al., 2013](#); [Stancescu et al., 2015](#)).

Microelectrode array (MEA) measurements

MEAs for neuronal plating were prepared as described above to localize neuronal bodies on electrodes, with process extension between upper and lower electrodes to allow synapse formation. MEAs for cardiac activity measurements were prepared as described above to create a u-pattern connecting all the electrodes to allow conduction velocity measurements at various points along the pattern. Flexible elastomeric connectors (zebra connectors, FUJIPOLY) were placed into their respective slots in the multi-organ system housings with one end in contact with the electrode pads on the MEAs, with the opposite end coming in contact with a printed circuit board (PCB), to allow recording and stimulation of MEA electrodes via a commercially available Intan. Spontaneous action potential events from populations of preBötC neurons on each electrode were recorded for 2 min, cardiac spontaneous activity was recorded for 30 s followed by stimulation with 800 mV rectangular pulses at 0.5–3.0 Hz in 0.25 Hz increments for 100 s.

Testing schedule and dosing with compounds

MEAs and cantilevers were all tested one time at Day 6 to establish predose baseline values. At Day 7, systems were split up at random into 4 groups, control (vehicle control), methadone (Sigma, 1398009) only (20 nM), naloxone (Sigma, 1453005) only (10 μ M), and methadone plus naloxone. Control, methadone only, and naloxone only were tested by adding the corresponding compounds which were suspended in 600 μ L of MOSM, and administered to systems via both feeding ports, 300 μ L in each port. A spontaneous recording from the neuronal MEAs was taken immediately after dosing, after which the systems were placed back into the incubator onto a rocker set to a tilt setting of 6°, instead of the normal 1 degree, for 10 min to fast mix. Following the fast mixing, neuronal MEAs were recorded again, as well as the mentioned cardiac MEA, cardiac cantilever, and SKM recordings. For the methadone plus naloxone condition, systems were first dosed with methadone only, neuronal MEAs were recorded, then naloxone was administered followed by a second neuronal MEA recording, after which the systems were placed on the fast mixer. Following 10 min of fast mixing, a third recording was taken, this time from all the components, neuronal, cardiac, and SKM. After completion of testing, systems were disassembled and the components were assessed for endpoint assays.

Endpoint assays

Cytochrome p450 3A4 activity

Once systems were disassembled, hepatocyte coverslips were transferred to a 24-well plate (Thermo Fisher Scientific, 142475). Hepatocyte function was evaluated by measuring cytochrome p450 3A4 (CYP3A4) activity with a Promega P450-Glo CYP3A4 Assay (Promega, V9002) kit containing Luciferin-IPA and Luciferin Detection Reagent (LDR). Hepatocytes were rinsed thrice with 500 μ L of 1 x Phosphate Buffered Saline (PBS) (Gibco, 14190–144) followed by a 1 h incubator in a solution of 11.95 μ M Luciferin-IPA and 200 μ L of clear 1 x Dulbecco's Modified Eagle Medium (DMEM)/F-12 (Gibco, 21041–025) at 37 °C and 5 % CO_2 . Luciferin-IPA is a proluciferin that converts to luciferin upon CYP3A4 interaction. Sample solutions were then stored at –20 °C until CYP3A4 activity quantification.

For CYP3A4 activity quantification, 50 μ L of sample or Beetle D-luciferin standard (Promega, E1601), was incubated with 50 μ L of LDR

in a white opaque 96-well plate (Greiner, 655098) for 20 min at room temperature in the dark. Relative light unit (RLU) luminescence produced from LDR's reaction with luciferin was quantified using a Synergy HT plate reader (Bio-Tek) and Gen5 software (Bio-Tek). RLU readouts were scaled to the 100 nM standard, which was designated an 80,000 RLU value prior to luminescence reading. Luminescence was measured five times to verify stabilization of the plate reader's photomultiplier tube. RLU sample averages were plotted on a standard curve (1–1000 nM range of Beetle D-luciferin) followed by a numerical conversion of nM hepatocyte D-luciferin to pmol D-luciferin/h/10⁶ cells.

Cell Viability

Hepatocyte viability was determined through an MTT (3-(4,5-Dimethylthiazol-2-yl)-2,5-diphenyltetrazolium bromide) assay. Once sample solutions from hepatocyte coverslips were stored for CYP3A4 activity quantification, hepatocytes were incubated for 1 h in a solution of 1.1 mM MTT (Thermo Fisher Scientific, M6494) and 500 μ L of clear Hepatocyte Culture Medium (PhoenixSongs, HCM500) at 37 °C and 5 % CO₂. To dissolve formazan crystal products, the MTT solution was discarded and hepatocytes were incubated with a 200 μ L dimethyl sulfoxide (DMSO) (Sigma-Aldrich, D4540) solution comprising 10 % sodium dodecyl sulfate (SDS) (Sigma-Aldrich, 151–21-3) and 0.5 % acetic acid (Sigma-Aldrich, A6283) for 10 min at room temperature on a shaker (OxfordLP Benchmate S4P-D) (300 rpm). 100 μ L of solution was then dispensed in a 96-well plate (Corning, 3595) and absorbance was read using a Synergy HT plate reader and Gen5 software at 570 nm.

PreBötC, cardiac and skeletal muscle cell viability was measured using Alamar blue (Thermo Fisher Scientific, DAL1100). After system disassembly, MEA-plated preBötC cells were placed in a 6-well plate (Corning, 353846) and incubated in 2 mL of NMJ 50:50 medium containing a 10 % v:v solution of Alamar blue. Cantilever-plated cardiac and skeletal muscle cells were placed in a 12-well plate (Greiner, 665180) and incubated in 1 mL of NMJ 50:50 medium containing a 10 % v:v solution of Alamar blue. Cells were then incubated for 48 h at 37 °C and 5 % CO₂. 100 μ L of solution was then dispensed in a 96-well plate and fluorescence (570 nm excitation, 590 nm emission) was read with a Synergy HT plate reader and Gen5 software.

Results

Multi-organ system design

The multi-organ system utilized for this study is a previously described gravity driven, customizable platform (McAleer et al., 2019; Oleaga et al., 2016, 2019). The top and bottom housings were fabricated using polymethyl methacrylate, with poly(dimethylsiloxane) (PDMS) gaskets in between to hold the bioMEMS chips in place as well as create a flow path for the multi-organ system medium (MOSM). The design was determined using computational fluid dynamic modeling (CFD), to determine rocking speed, component area dimensions, shear stresses, and flow rates (Fig. 1B) (McAleer et al., 2019; Miller and Shuler, 2016; Oleaga et al., 2016). For this study, the multi-organ platform consisted of 4 cell types, hepatocytes, cardiomyocytes, skeletal muscle (SKM), and preBötzing complex neurons (preBötC) which were all plated individually in their own respective medium to mature before being assembled into the multi-organ housing. The placement of each component within the system is shown in Fig. 1, with the hepatocyte component being the first component, located immediately following the inlet reservoir to ensure any compound added to the system would be metabolized, as previously shown (Oleaga et al., 2021). Following the hepatocyte component, are the two cantilever devices, one seeded with cardiomyocytes, and another seeded with SKM to allow collection of contractile force data. MEAs were placed at the end of the system, one MEA seeded with cardiomyocytes to collect conduction velocity and mISI, and the other MEA seeded with preBötC neurons to collect spontaneous firing of action potentials.

Characterization of organ components

Prior to assembly or testing of the multi-organ systems, the individual cell types were characterized for opioid receptor expression via immunocytochemistry (ICC) under flow conditions (Fig. 2). Since methadone is known to primarily act on μ -opioid receptors, it was one of the 3 opioid receptors that was stained for, as well as δ and κ opioid receptors (Prommer et al., 2021). Preliminary ICC indicated robust expression of μ -opioid receptors for all 4 of the organs in static conditions, δ -opioid receptor expression appeared mostly in hepatocytes, and κ -opioid expression was seen in hepatocytes, skeletal muscle, and preBötC neurons (Supp. Fig. 1). However, when the same ICC was performed after exposure to flow conditions, the expression of δ -opioid

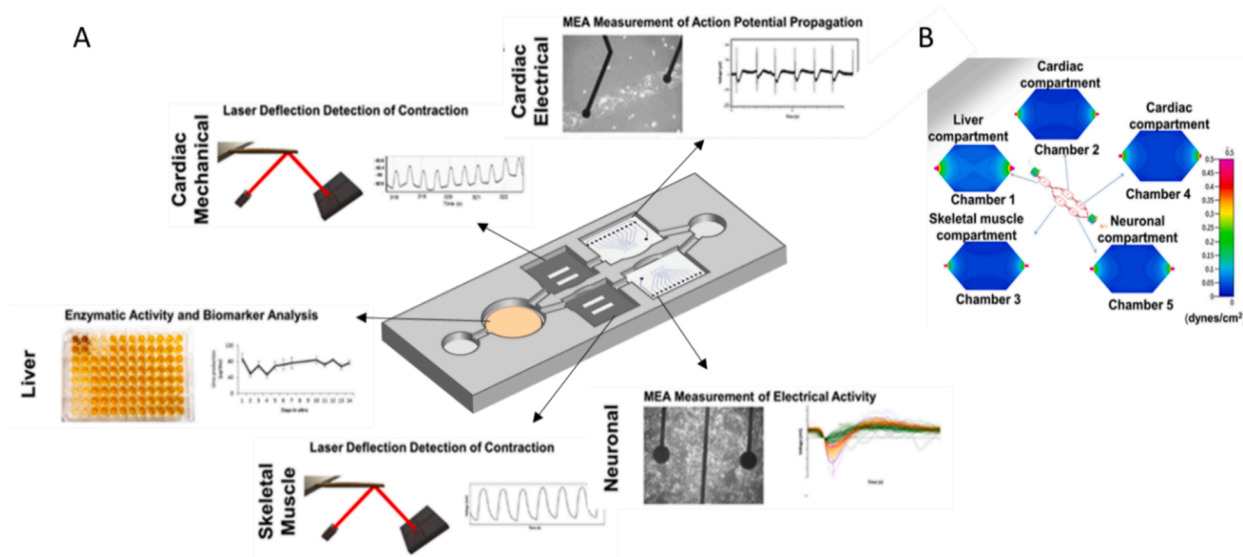


Fig. 1. Schematic and layout of multi-organ system. A) Schematic of multi-organ system with examples of functional components, B) CFD model showing fluid shear stress throughout the multi-organ system.

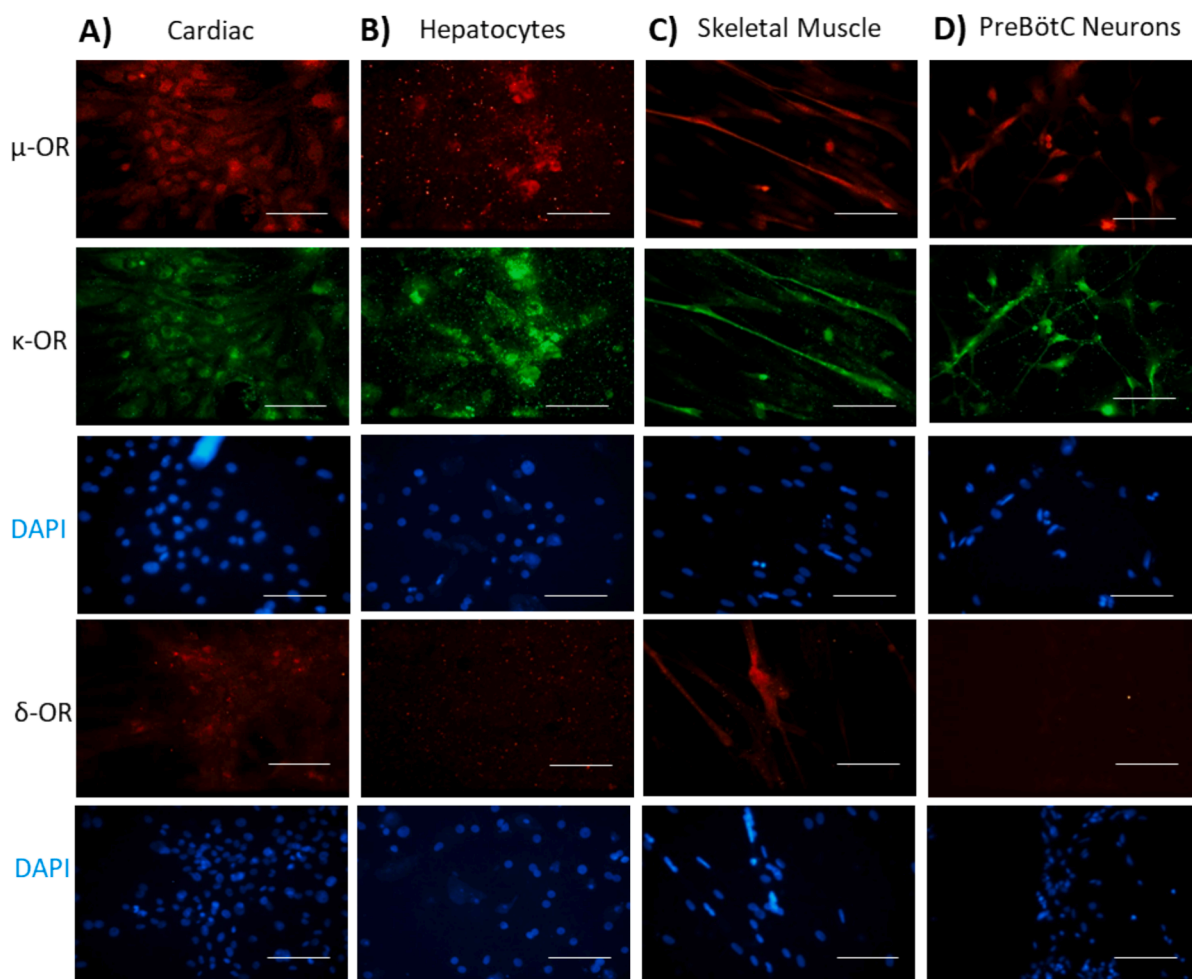


Fig. 2. Immunocytochemical characterization of opioid receptor expression of the multi-organ system components under flow condition. A) opioid receptor expression of cardiomyocytes, B) opioid receptor expression of hepatocytes, C) opioid receptor expression of skeletal muscle, D) opioid receptor expression of preBötC neurons; scale bars = 100μm.

receptors on hepatocytes appeared to be reduced, while skeletal muscle saw an increase of this receptor expression, and both δ - and κ -opioid expression was seen in cardiomyocytes, which correlates with expression patterns seen *in vivo*, suggesting the need for flow conditions to more accurately represent conditions in the human body (Evans and Smith, 2004) (Fig. 2). Toll-like receptor 4 (TLR4) expression was also stained for as this receptor family has been implicated to be active in the transmission and retention of chronic pain, and therefore has been investigated as a potential off-target interaction of opioid drugs (Supp. Fig. 2) (Hutchinson et al., 2007; Zare et al., 2023).

In order to confirm the metabolic capability of the hepatocytes, hepatocytes alone were dosed with the synthetic opioid methadone, and the concentration of the parent compound and resulting metabolites were measured via high performance liquid chromatography mass spectrometry (HPLC-MS). Hepatocytes were dosed with 10 μ M methadone, and samples were collected and analyzed at 6, 12-, 24-, 36-, and 48-hour time points. The concentration of the parent compound methadone was seen to decrease from 10.313 μ M at 6 h, to 9.070 μ M at 48 h. As the amount of parent compound decreased, an increase in the metabolites of methadone, 2-ethyl-5-methyl-3,3-diphenylpyrrolidine (EDDP) and 2-ethyl-5-methyl-3,3-diphenylpyrroline (EMDP), were seen to increase in the same timeframe with the greatest increase observed in EDDP from 0.373 μ M at 6 h to 5.103 μ M at 48 h confirming the metabolic capacity of the hepatocytes (Supp. Fig. 3).

All cell types were plated onto their respective surfaces in their own maturation medium and allowed to mature for 7 days before assembly

into the multi-organ system. On the day prior to beginning the assembly process, all the individual components were imaged via phase microscopy to ensure cell viability, as well as proper cell patterning on the MEAs (Supp. Fig. 4). Once the quality of the organ components was confirmed, they were assembled into the multi-organ system housings in a common medium, MOSM, at an osmolarity of 300 mOsm (MOSM high).

Assembly and testing of multi-organ systems

Each of the components, hepatocyte coverslip, cardiac and skeletal muscle cantilevers, and cardiac and preBötC MEAs, were assembled into the systems using MOSM. Systems were fed daily by removing 600 μ L of medium from the end reservoir and replenished with the same volume of medium into the reservoir closest to the liver with MOSM at an osmolarity of 260 mOsm (MOSM 50:50). The hepatocyte component was the first organ in the OoaC system, allowing it to metabolize any compounds introduced into the system, allowing interaction of the compound metabolites with the rest of the organ components. After assembly, systems were maintained for 1 week without any dosing or testing in order to allow the cells to acclimate to the MOSM, as well as continue maturation. To maintain consistent flow and medium exchange, systems were stored on a rocker set to 1° tilt, at a speed of 1 tilt per minute in a 37 °C incubator, causing gravity driven flow as opposed to using a pump system utilized by some traditional multi-organ OoaC platforms, offering the advantage of not requiring tubing or pumps, saving space, while

also reducing the risk of bubble formation within the system (Khalid et al., 2017; Driver and Mishra, 2023; Sung et al., 2010). 6 days after systems were assembled, each of the components were imaged to confirm the cells were still viable for functional testing (Fig. 3). Once viability was confirmed, each of the components within the systems were tested to establish baseline function for each of the platforms.

After baseline values were collected at Day 6, overdose and recovery testing was done the following day at Day 7. Systems were randomly split into 4 dosing conditions, vehicle control, methadone only, naloxone only, and methadone followed by rescue with naloxone. For the control, methadone only, and naloxone only conditions, the system was dosed, and the spontaneous activity of the preBötCs was immediately recorded (Test 1). After the initial recording, systems were placed on a rocker set at a speed of 1, tilt at 6°, in a 37 °C incubator for 10 min for fast mixing to ensure even distribution of the dosed substance across all the components in the multi-organ platform. Following the 10-minute fast mix, all the components including the preBötC MEA (Test 2), cardiac MEA, skeletal muscle cantilever, and cardiac cantilever were tested. The methadone + naloxone condition was tested in a similar manner, with one additional step due to the addition of the second substance, naloxone. For these systems, methadone was dosed and the preBötC MEA was recorded immediately (Test 1*), after which naloxone was dosed, and the preBötC MEA was recorded again (Test 2*). After the second recording, the system was placed on the fast mix rocker for 10 min prior to testing all the components (Test 3*) (Supp. Fig. 6). After all systems had been tested, they were imaged to confirm cell attachment and viability before disassembly for endpoint viability assays (Supp. Fig. 5).

The preBötC component was used to indicate the occurrence of an overdose event. As expected, control and naloxone systems showed no significant change in the amount of spontaneous activity confirming that there was no effect from the vehicle control or naloxone only (Fig. 4A,B). Methadone however, showed a significant decrease in spontaneous firing of preBötCs immediately after dosing, which continued after the fast mixing (Fig. 4C). In the overdose followed by recovery condition, a significant reduction in spontaneous activity after methadone dosing was observed, followed by recovery after naloxone was administered. After the 10-minute fast mixing, a significant increase in the preBötC spontaneous activity was witnessed compared to after methadone dosing, returning to the same level as predose activity (Fig. 4D).

Cardiac measurements were collected using both a cardiac MEA and cantilever in each system. Cardiac MEAs were used to determine conduction velocity from one electrode to the next on the patterned cardiomyocytes, as well as the minimal inter-spike interval (mISI), a correlate to QT interval (Fig. 5A, B). Cardiac cantilevers allowed collection of contractile force, or amplitude, as well as beat frequency.

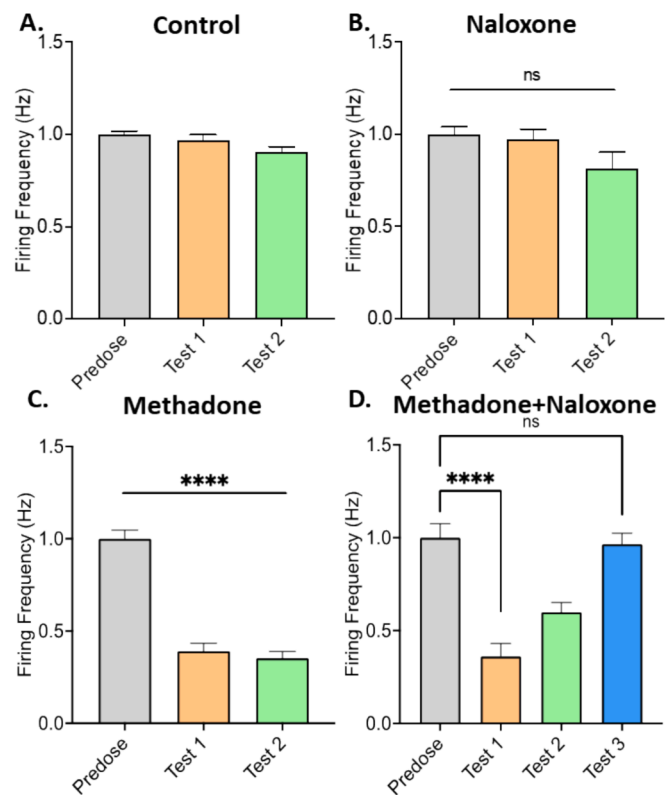


Fig. 4. PreBötC neuron spontaneous firing frequency. A) spontaneous firing in response to dosing with vehicle control, B) spontaneous firing in response to naloxone, C) spontaneous firing in response to methadone dosing, D) spontaneous firing in response to methadone dosing, followed by naloxone administration and circulation; data collected from more than 3 independent biological replicates per condition, data is shown as mean normalized to predose, following a blocking for system. Error bars indicate SEM; One-way ANOVA followed by Tukey's test: Naloxone- $P^{n.s.} = 0.1$; Methadone- predose vs test 1, $P^{****} < 0.0001$, predose vs test 2, $P^{****} < 0.0001$; Methadone + Naloxone- predose vs test 1, $P^{****} < 0.0001$, test 1 vs test 3, $P^{****} < 0.0001$, predose vs test 3, $P^{n.s.} = 0.9$.

Interestingly, a significant reduction was seen in the cardiac beat frequency, contractile force, and mISI, in response to naloxone only dosing, while a significant increase was observed in the methadone followed by naloxone rescue condition, suggesting naloxone may be causing off-target effects on the cardiomyocytes (Fig. 5D).

Skeletal muscle function was investigated using cantilevers to collect

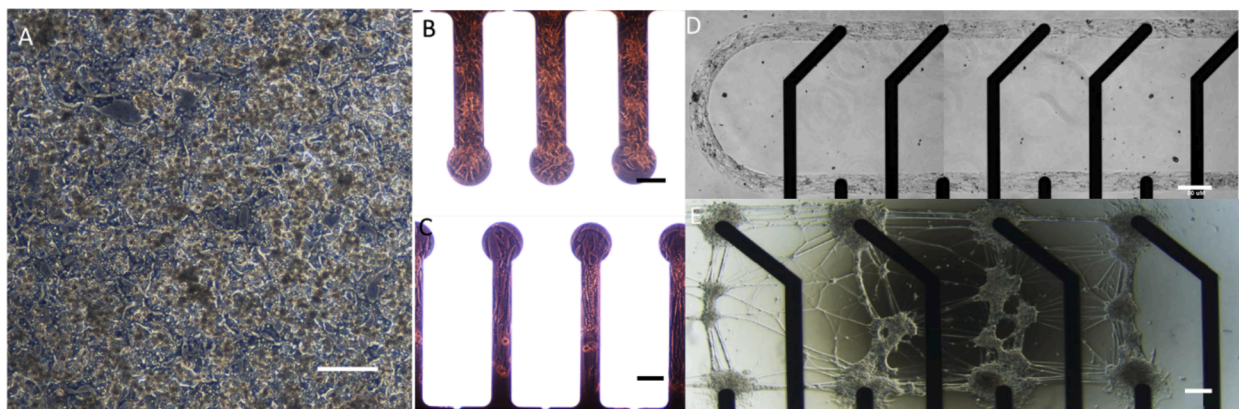


Fig. 3. Phase images of organ components inside the multi-organ system. A) hepatocytes after assembly into the multi-organ system, B) cardiomyocyte cantilevers after assembly into multi-organ system, C) skeletal muscle cantilevers after assembly into the multi-organ system, D) patterned cardiomyocyte MEA after assembly into the multi-organ system, E) patterned preBötC MEA after assembly into the multi-organ system; scale bars = 50μm.

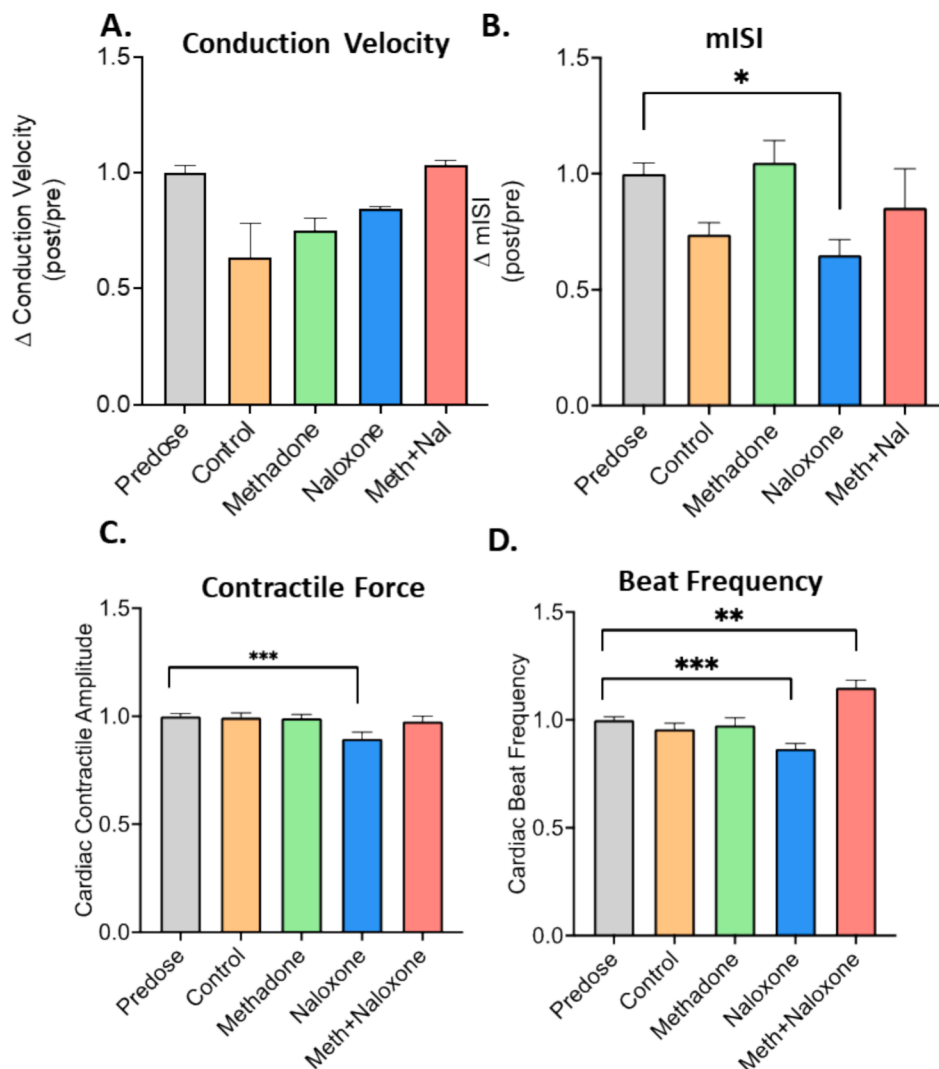


Fig. 5. Cardiac function on MEAs and cantilevers. A) cardiac conduction velocity on patterned MEAs, B) cardiac mISI on patterned MEAs, C) cardiac contractile force on cantilevers, D) cardiac beat frequency on cantilevers; data collected from more than 3 independent biological replicates per condition, data is shown as mean normalized to predose, following a blocking for system. Error bars indicate SEM; One-way ANOVA followed by Tukey's test: mISI- predose vs Naloxone $P^* = 0.04$, predose vs control $P^{n.s.} = 0.2$; Contractile force- predose vs Naloxone $P^{***} = 0.0007$; Beat Frequency- predose vs Naloxone $P^{****} = 0.0004$, predose vs Methadone + Naloxone $P^{**} = 0.002$.

contractile force, or amplitude, of myotube contractions in response to electrical stimulation. While not significant, what appears to be a slight increase in contractile force was observed in response to methadone only dosing compared to predose, ($P^{n.s.} = 0.082$) with no significant differences in any of the other conditions (Fig. 6A). While further investigation would be required, this is an interesting trend that could potentially be due to an increase in release of intracellular Ca^{2+} stores due to opioid receptor activation, a G protein coupled receptor pathway (Harrison et al., 1998). Hepatocyte enzymatic function was determined after systems were disassembled via a CYP3A4 assay, which indicated no significant change in CYP activity in any of the conditions (Fig. 6B).

Viability endpoint assays

After completion of Day 7 acute overdose induction and testing, systems were disassembled to assess viability. An Alamar Blue viability assay was performed on cardiac cantilevers, skeletal muscle cantilevers, and neuronal MEAs, while a MTT assay was utilized for hepatocytes as the collagen hydrogel on the hepatocytes is prohibitive for Alamar Blue. While slight variations were observed for some of the cells and conditions, no significant difference was detected (Fig. 7).

Discussion

Here we demonstrate the utilization of a microphysiological system to model acute opioid overdose and recovery. Consisting of cardiac, skeletal muscle, preBötC neurons, and hepatocytes, this multi-organ platform enabled investigation of functional effects of the opioid methadone and rescue agent naloxone. Opioid receptors are G-protein coupled receptors, with μ , κ , and δ being the major opioid receptor subtypes. While opioids can act on all three of these receptors, the μ opioid receptor is the most widely expressed opioid receptor, making it the most common target upon which most opioids act. It has also been suggested to be involved in activating central dopamine reward pathways, which can lead to the risk of abuse and subsequent addiction to opioids (Al-Hasani and Michael, 2011). Before any multi-organ experiments were conducted, opioid receptor expression was characterized for all the organ components under flow via ICC to investigate which organ components exhibited targets for opioid binding (Fig. 2). The ICC indicated expression of μ and κ opioid receptors on all the cell types, while skeletal muscle and cardiomyocytes exhibited robust δ opioid receptor expression in addition to μ and κ opioid receptor expression when placed in flow conditions. Previous in vivo studies have shown expression of all

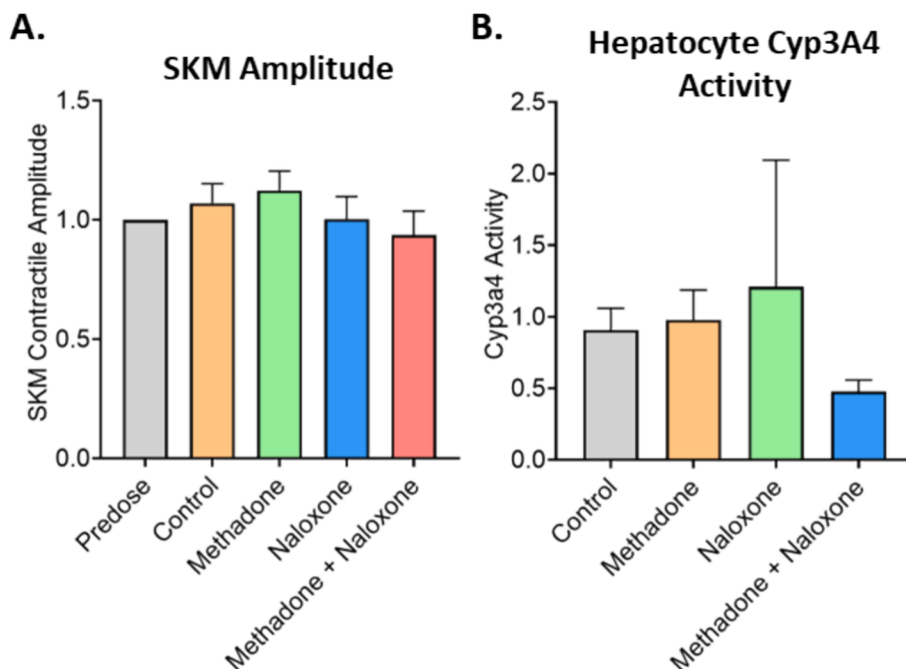


Fig. 6. Skeletal muscle contractile force and hepatocyte enzymatic activity. A) skeletal muscle amplitude on cantilevers, B) no significant change was observed in hepatocyte enzymatic activity; data collected from more than 3 independent biological replicates per condition, data is shown as mean with error bars indicating SEM.

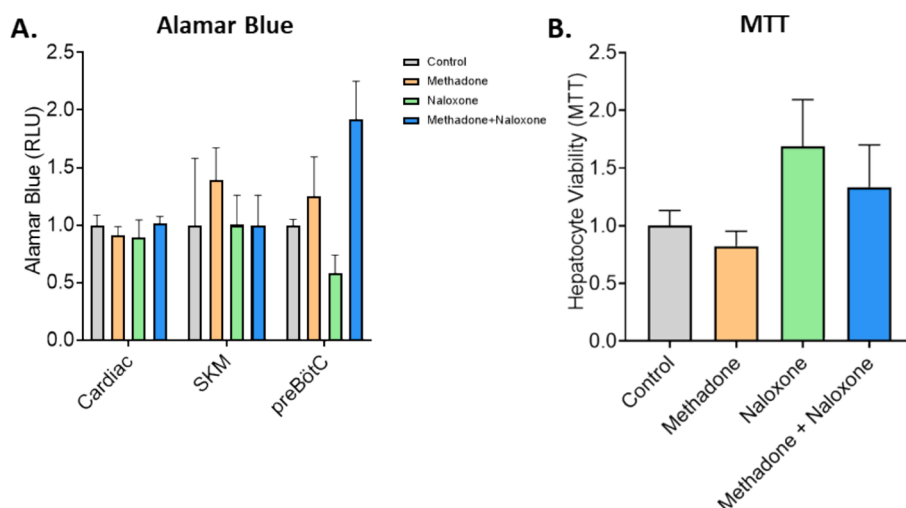


Fig. 7. Viability assays. A) Cardiac, SKM, and preBötC viability determined via Alamar Blue, B) hepatocyte viability determined via MTT (control: gray, methadone: orange, naloxone: green, methadone + naloxone: blue). (For interpretation of the references to colour in this figure legend, the reader is referred to the web version of this article).

three opioid receptors in cardiac tissue, as well as skeletal muscle which aligns with our findings (Evans et al., 1995; Evans and Smith, 2004; Sobanski et al., 2014). However, there was some difference noted when the same staining was performed in static conditions, suggesting that the flow conditions more accurately mimicked those seen in vivo (Supp. Fig. 1). Toll-like receptor 4 is a receptor that is well known for its role in proinflammatory response induction and was also evaluated as some studies have shown that opioids can also bind to this receptor. Robust expression of TLR4 was observed in skeletal muscle and preBötC neurons (Fig. 2C, D). While this receptor has typically been implicated in infectious diseases, some studies have shown that it may also be activated by opioids, as well as contribute to drug addiction (Hutchinson et al., 2010; Molteni et al., 2016; Wu and Li, 2020). When opioids are present in the absence of lipopolysaccharide (LPS), they can bind to

TLR4, activating that signaling pathway, which in turn can lead to an increase of MAPK signaling, potentially providing an additional pathway which opioids and opioid receptor antagonists may activate (Zhang et al., 2020). This provides an alternate target for further study utilizing these systems.

The multi-organ system described here proffers the advantage of the ability to collect functional data from the organ components in addition to biomarker readouts. Since the liver is the organ responsible for metabolism of compounds introduced to the body, the metabolic function of our hepatocyte component was confirmed before multi-organ experiments were performed. Methadone was added to hepatocyte only coverslips, and the concentration of the parent compound and metabolites was investigated via HPLC-MS. Methadone is a synthetic opioid which is metabolized into two main metabolites EMDP and EDDP

(Sporkert and Pragst, 2000). Analysis of these compounds saw a decrease in the parent compound methadone, with an increase in both EDDP and EMDP over the course of 48 h, suggesting active metabolism of methadone by the hepatocytes (Supp. Fig. 3).

Following ICC characterization of opioid receptors and methadone metabolism, organ components were assembled into multi-organ systems for collection of functional readouts and biomarkers from the 4 organ types. Attachment and viability of cells was confirmed via phase microscopy one day after assembly into multi-organ systems (Supp. Fig. 4), prior to baseline testing at Day 6 (Fig. 3), and following dosing and testing at Day 7 (Supp. Fig. 5). Functional readouts included contractile force, spontaneous beat frequency, conduction velocity (a QT interval analog referred to as mISI) from cardiac cells, contractile force from skeletal muscle, frequency of action potential firing for preBötC neurons, and CYP3A4 activity for hepatocytes. Testing in the multi-organ systems was performed at Day 6 with no compounds administered to the systems to establish baseline function, and the following day, systems were split into four dosing conditions, vehicle control, methadone only, naloxone only, and methadone followed by naloxone for recovery. Dosing concentration was determined based on the dose response curve collected by Guo et al., 2024. For methadone, the curve was utilized to determine a dosing concentration that caused a greater than 50 % decrease in PreBötC activity without completely abolishing firing activity as this is what has been seen to occur in previous *in vivo* studies (Ramirez et al., 2021; Guo et al., 2024). Using this information 10 μ M was determined as the dosing concentration for naloxone, as this is where peak recovery was observed by Guo et al., 2024.

Functional values at Day 7 were normalized to baseline Day 6 values to determine fold change, if any, for each of the functional readouts. Electrical activity of the preBötC neurons was tested using MEAs and primarily utilized as an indicator for the occurrence of an overdose event. The PreBötzing complex has been widely characterized as one of the main targets of opioid overdose, as it plays an integral role in the maintenance of respiratory function (Hayes et al., 2012; Wang et al., 2014). Opioids cause a phenomenon referred to as opioid induced respiratory depression (OIRD), which is thought to be induced by inhibition of rhythmic respiration, a function controlled by the preBötzing complex (Bachmutsky et al., 2020). Of the three classes of opioid receptors, the μ opioid receptor is the primary opioid receptor mediating OIRD, the expression of which was observed on the preBötC neurons utilized in the multi-organ system (Dahan et al., 2001, 2010). When dosed with the vehicle control and naloxone only, no significant change was observed in the frequency of spontaneous firing, while methadone administration caused a significant decrease in the firing frequency, with a reduction of ~ 60 %, suggesting the occurrence of an opioid overdose event (Fig. 4). When naloxone was administered immediately following an overdose event, firing frequency was restored to that of baseline predose levels, indicating efficient rescue following an opioid overdose (Fig. 4D).

Cardiac function, both electrical and mechanical, was collected through the use of both MEAs and cantilevers. Electrical readouts from MEAs included changes in conduction velocity and mISI. Conduction velocity measurements were performed on patterned MEAs by stimulating one electrode and measuring the time between initial stimulation and action potential firing on the adjacent electrode, and mISI was used as a QT interval analog, collected as described in Stancescu et al. (Stancescu et al., 2015). Mechanical readouts included changes in contractile force and spontaneous beat frequency collected using cantilevers. While no significant changes were observed in conduction velocity, significant changes were observed in cardiac beat frequency, with a reduction in the naloxone condition, and an increase in methadone followed by naloxone condition, as well as a reduction in both mISI and contractile force in response to naloxone only (Fig. 5). Previous studies utilizing guinea pig isolated atria have shown naloxone at concentrations of 1.5 to 120 μ M can cause a reduction in beat frequency, which aligns with the data collected from cardiac cells in the multi-organ

system (Brasch, 1986). Clinical case studies regarding patients admitted to the hospital for receiving high doses of opioids treated with naloxone administration has seen occurrence of ventricular tachycardia, which potentially correlates to the increase in beat frequency seen in the methadone overdose followed by naloxone rescue condition in our system (Lameijer et al., 2014).

Skeletal muscle function consisted of contractile force, which was also collected using cantilevers. While no significant effect on contractile force was observed, methadone only did cause what appears to be a slight increase in contractile force (Fig. 6A). While muscle rigidity is a known side effect of synthetic opioid use, it has mostly been attributed to being a result of μ opioid receptor binding of neurons to the dopaminergic pathway in the CNS (Buxton JA, Gauthier T, Kinshella MW, Godwin J., 2018; Radke et al., 2014; Rosal et al., 2021). However, the skeletal muscle in our multi-organ system was not innervated by any neurons, suggesting that opioid binding to the skeletal muscle itself may be contributing to this rigidity by potentially directly increasing contractile force. Activation of μ opioid receptors by methadone has been seen to block K^+ channels, and other studies have demonstrated that blockade of K^+ channels improved contractile performance in skeletal muscle (Kokate and Frank, 1989; Matsui and Williams, 2010; van Lunteren and Moyer, 2012; van Lunteren and Pollarine, 2010). Opioid receptors are G-protein coupled receptors, a class of receptors with a wide range of secondary signaling pathways. One of these pathways is the adenylyl cyclase-cAMP pathway, which can activate PKA, leading to an increase in release of intracellular calcium (Harrison et al., 1998). Since the binding of myosin to actin is dependent on troponin C bound calcium ions, skeletal muscle force is directly correlated to the calcium concentration (Gehlert et al., 2015). Further investigation would be required, however, as while skeletal muscle rigidity in opioid overdose has mainly been attributed to dysfunction in the CNS caused by μ -opioid receptor binding, the data shown here may suggest that the skeletal muscle itself could also be contributing to this side effect, independent of its neuronal innervation.

Hepatocyte function was determined after testing was complete, via a CYP3A4 assay. This particular enzyme was chosen for analysis as it is one of the most important hepatic cytochromes involved in drug metabolism (Wilkinson, 1996). No significant difference in enzymatic activity was discerned in any of the conditions, suggesting the metabolic ability of the liver component was not affected by methadone, naloxone, or a combination of both (Fig. 6B). After the conclusion of experiments, systems were disassembled to investigate the viability of the cells in response to either of the compounds. Alamar blue was utilized for the neuronal MEAs, cardiac cantilevers, and skeletal muscle cantilevers. For the liver, a MTT (3-(4,5-dimethylthiazol-2-yl)-2,5-diphenyltetrazolium bromide) assay was utilized, as this is a metabolic activity-based viability assay (Ghasemi et al., 2021). Viability assays showed no significant differences between control systems and those dosed with methadone or naloxone, confirming that any functional differences observed were not due to cell death in the system.

Conclusion

In this work we have described the establishment of a human cell-based model of opioid overdose utilizing an organ-on-a-chip multi-organ platform. Consisting of preBötzing complex neurons, cardiac, skeletal muscle, and liver components, this system allowed investigation of the effects of the synthetic opioid methadone, as well as a commonly recognized overdose first response treatment agent, naloxone. The specific model of opioid overdose described here has the potential to provide a method for rapidly screening newly developed treatments for opioid overdose. Additionally, by performing longer lasting chronic experiments, in future studies long term effects of repeated opioid overdose, and the efficacy of naloxone in those situations could also be investigated. Such an opioid overdose model is especially relevant in current times due to the number of deaths occurring due to the opioid

epidemic. Many fentanyl related overdoses also involve additional drugs such as amphetamines due to laced street drugs, providing another important potential application of this organ-on-a-chip platform to assist improvement of treatment strategies for such co-administered drug related overdoses. As the pharmaceutical industry starts to shift from animal models to human based in vitro platforms, multi-organ systems like the one described here will provide highly useful tools for investigation of both drug efficacy and off-target toxicity in a cost effective and efficient manner.

Declaration of competing interest

The authors confirm that competing financial interests exist but there has been no financial support for this research that could have influenced its outcome.

James J Hickman reports a relationship with Hesperos, Inc. that includes: board membership and equity or stocks. If there are other authors, they declare that they have no known competing financial interests or personal relationships that could have appeared to influence the work reported in this paper.

Acknowledgements

Funding: This work was funded by the National Institutes of Health grant # NIH_NOA_1UG3TR003081.

Author contributions: AP, SP, XG, MS, SS, PT and JJH conceived and designed the experiments; AP, SP, HW, CD, JG, DN, SL, AC, XG, PK, JR, WB, and JK performed the experiments; AP, SP, DN, SL, CL, XG, JK, SS, PT, and JJH analyzed the data; AP and JJH prepared the manuscript.

Appendix A. Supplementary material

Supplementary data to this article can be found online at <https://doi.org/10.1016/j.crtox.2024.100209>.

Data availability

Data will be made available on request.

References

- Al-Hasani, R., Michael, R., 2011. Bruchas, molecular mechanisms of opioid receptor-dependent signaling and behavior. *Anesthesiology* 115 (6), 1363–1381.
- Bachmutsky, I., Wei, X.P., Kish, E., Yackle, K., 2020. Opioids depress breathing through two small brainstem sites. *Elife* 9, e52694.
- Barron, B.A., 1999. Opioid peptides and the heart. *Cardiovasc. Res.* 43 (1), 13–16.
- Bateman, J.T., Saunders, S.E., Levitt, E.S., 2023. Understanding and countering opioid-induced respiratory depression. *Br. J. Pharmacol.* 180 (7), 813–828.
- Boyella, V.D., Nicastri, A.D., Bergasa, N.V., 2008. Human hepatic met-enkephalin and delta opioid receptor-1 immunoreactivities in viral and autoimmune hepatitis. *Ann. Hepatol.* 7 (3), 221–225.
- Brasch, H., 1986. Influence of the optical isomers (+) and (–)-naloxone on beating frequency, contractile force and action potentials of guinea-pig isolated cardiac preparations. *Br. J. Pharmacol.* 88 (4), 733–740.
- Buxton, J.A., Gauthier, T., Kinshella, M.W., Godwin, J., 2018. A 52-year-old man with fentanyl-induced muscle rigidity. *Can. Med. Assoc. J.* 190 (17), E539–E541.
- Campbell, N.D., 2019. Naloxone as a technology of solidarity: history of opioid overdose prevention. *CMAJ* 191 (34), E945–E946.
- Chhatwal, J., Mueller, P.P., Chen, Q., Kulkarni, N., Adey, M., Zarkin, G., LaRochelle, M. R., Knudsen, A.B., Barbosa, C., 2023. Estimated reductions in opioid overdose deaths with sustainment of public health interventions in 4 US States. *JAMA Netw. Open* 6 (6), e2314925.
- Dahan, A., Aarts, L., Smith, T.W., 2010. Incidence, reversal, and prevention of opioid-induced respiratory depression. *Anesthesiology* 112 (1), 226–238.
- Zhang, P., Yang, M., Chen, C., Liu, L., Wei, X., Zeng, S., 2020. Toll-Like receptor 4 (TLR4)/opioid receptor pathway crosstalk and impact on opioid analgesia, immune function, and gastrointestinal motility. *Front. Immunol.* 11.
- Cook D, Brown D, Alexander R, March R, Morgan P, Satterthwaite G, Pangalos MN. Cook, D., 2014. Lessons learned from the fate of AstraZeneca's drug pipeline: a five-dimensional framework. *Nat. Rev. Drug Discov.* 13 (6), 419–431.
- Dasgupta, A., Chapter 2 - Prescription Opioids: An Overview, in *Fighting the Opioid Epidemic*, A. Dasgupta, Editor. 2020, Elsevier. p. 17–41.
- Dahan, A., Sarton, E., Teppema, L., Olivevier, C., Nieuwenhuijs, D., Matthes, H.W., Kieffer, B.L., 2001. Anesthetic potency and influence of morphine and sevoflurane on respiration in μ -opioid receptor knockout mice. *Anesthesiology* 94 (5), 824–832.
- Driver, R., Mishra, S., 2023. Organ-on-a-chip technology: an in-depth review of recent advancements and future of whole body-on-chip. *BioChip J.* 17 (1), 1–23.
- Evans, A.A.L., Hughes, S., Smith, M.E., 1995. Delta-opioid peptide receptors in muscles from obese diabetic and normal mice. *Peptides* 16 (2), 361–364.
- Evans, A.A., Smith, M.E., 2004. Opioid receptors in fast and slow skeletal muscles of normal and dystrophic mice. *Neurosci. Lett.* 366 (3), 339–341.
- Friedman, J., Gjersing, L., 2023. Increases in drug overdose deaths in Norway and the United States during the COVID-19 pandemic. *Scand. J. Public Health* 51 (1), 53–57.
- Gehlert, S., Bloch, W., Suhr, F., 2015. Ca²⁺-dependent regulations and signaling in skeletal muscle: from electro-mechanical coupling to adaptation. *Int. J. Mol. Sci.* 16 (1), 1066–1095.
- Guo, X., Akanda, N., Fiorino, G., Nimbalkar, S., Long, C.J., Colón, A., Patel, A., Tighe, P. J., Hickman, J.J., 2024. Human IPSC-Derived PreBötC-Like Neurons and Development of an Opiate Overdose and Recovery Model. *Advanced Biology(Weinh.)*. Aug;8(8): e2300276.
- Ghasemi, M., Turnbull, T., Sebastian, S., Kempson, I., 2021. The MTT assay: utility, limitations, pitfalls, and interpretation in bulk and single-cell analysis. *Int. J. Mol. Sci.* 22 (23).
- Guo, X., Badu-Mensah, A., Thomas, M.C., McAleer, C.W., Hickman, J.J., 2020. Characterization of functional human skeletal Myotubes and neuromuscular junction derived—from the same induced pluripotent stem cell source. *Bioengineering* 7 (4), 133.
- Harrison, C, Smart, D, Lambert, D.G., 1998. Stimulatory effects of opioids Br. J. Anaesth. 81, 20–28.
- Hayes, J.A., Wang, X., Del Negro, C.A., 2012. Cumulative lesioning of respiratory interneurons disrupts and precludes motor rhythms in vitro. *Proc. Natl. Acad. Sci.* 109 (21), 8286–8291.
- Hughes, B., 2008. 2007 FDA drug approvals: a year of flux. *Nat. Rev. Drug Discov.* 7 (2), 107–109.
- Hutchinson, M.R., Bland, S.T., Johnson, K.W., Rice, K.C., Maier, S.F., Watkins, L.R., 2007. Opioid-induced glial activation: mechanisms of activation and implications for opioid analgesia, dependence, and reward. *ScientificWorldJournal* 7, 98–111.
- Hutchinson, M.R., Zhang, Y., Shridhar, M., Evans, J.H., Buchanan, M.M., Zhao, T.X., Slivka, P.F., Coats, B.D., Rezvani, N., Wieseler, J., Hughes, T.S., Landgraf, K.E., Chan, S., Fong, S., Phipps, S., Falke, J.J., Leinwand, L.A., Maier, S.F., Yin, H., Rice, K. C., Watkins, L.R., 2010. Evidence that opioids may have toll-like receptor 4 and MD-2 effects. *Brain Behav. Immun.* 24 (1), 83–95.
- Khalid, N., Kobayashi, I., Nakajima, M., 2017. Recent lab-on-chip developments for novel drug discovery. *Wires Syst. Biol. Med.* 9 (4), e1381.
- Kokate, T.G., Frank, G.B., 1989. Blockade of K⁺ contractures in skeletal muscle by opioid drugs: a nonstereospecific effect. *Can. J. Physiol. Pharmacol.* 67 (5), 435–441.
- Lameijer, H., Azizi, N., Ligtenberg, J.J., Ter Maaten, J.C., 2014. Ventricular tachycardia after naloxone administration: a drug related complication? Case report and literature review. *Drug Saf Case Rep* 1 (1), 2.
- Matsui, A., Williams, J.T., 2010. Activation of μ -opioid receptors and block of Kir3 potassium channels and NMDA receptor conductance by L- and D-methadone in rat locus coeruleus. *Br. J. Pharmacol.* 161 (6), 1403–1413.
- McAleer, C.W., Long, C.J., Elbrecht, D., Sasserath, T., Bridges, L.R., Rumsey, J.W., Martin, C., Schnepfer, M., Wang, Y., Schuler, F., Roth, A.B., Funk, C., Shuler, M.L., Hickman, J.J., 2019. Multi-organ system for the evaluation of efficacy and off-target toxicity of anticancer therapeutics. *Sci. Transl. Med.* 11 (497), eaav1386.
- Miller, P.G., Shuler, M.L., 2016. Design and demonstration of a pumpless 14 compartment microphysiological system. *Biotechnol. Bioeng.* 113 (10), 2213–2227.
- FDA Modernization Act 2.0 S.5002 - 117th Congress. 2021–2022 [cited 2023 3/13]; Available from: <https://www.congress.gov/bill/117th-congress/senate-bill/5002>.
- Molteni, M., Gemma, S., Rossetti, C., 2016. The role of toll-like receptor 4 in infectious and noninfectious inflammation. *Mediators Inflamm.* 2016, 6978936.
- Oleaga, C., Bernabini, C., Smith, A.S., Srinivasan, B., Jackson, M., McLamb, W., Platt, V., Bridges, R., Cai, Y., Santhanam, N., Berry, B., Najjar, S., Akanda, N., Guo, X., Martin, C., Ekman, G., Esch, M.B., Langer, J., Ouedraogo, G., Cotovio, J., Breton, L., Shuler, M.L., Hickman, J.J., 2016. Multi-Organ toxicity demonstration in a functional human in vitro system composed of four organs. *Sci. Rep.* 6 (1), 20030.
- Oleaga, C., Bridges, L.R., Persaud, K., McAleer, C.W., Long, C.J., Hickman, J.J., 2021. A functional long-term 2D serum-free human hepatic in vitro system for drug evaluation. *Biotechnol. Prog.* 37 (1), e3069.
- Oleaga, C., Lavado, A., Riu, A., Rothenmund, S., Carmona-Moran, C.A., Persaud, K., Yurko, A., Lear, J., Narasimhan, N.S., Long, C.J., Sommerhage, F., Bridges, L.R., Cai, Y., Martin, C., Schnepfer, M.T., Goswami, A., Note, R., Langer, J., Teissier, S., Cotovio, J., Hickman, J.J., 2019. Long-term electrical and mechanical function monitoring of a human-on-a-chip system. *Adv. Funct. Mater.* 29 (8), 1805792.
- Prommer, E., P. Jacobs, and A.K. Mehta, Chapter 7 - Palliative Care and Cancer Pain, in *Pain Care Essentials and Innovations*, S. Pangarkar, Q.G. Pham, and B.C. Eapen, 2021, Elsevier. p. 91–111.
- Pirozzi, K.L., Long, C.J., McAleer, C.W., Smith, A.S., Hickman, J.J., 2013. Correlation of embryonic skeletal muscle myotube physical characteristics with contractile force generation on an atomic force microscope-based bio-microelectromechanical systems device. *Appl. Phys. Lett.* 103 (8).
- Radke, J.B., Owen, K.P., Sutter, M.E., Ford, J.B., Albertson, T.E., 2014. The effects of opioids on the lung. *Clin Rev Allergy Immunol* 46 (1), 54–64.
- Ramirez, J.M., Burgraff, N.J., Wei, A.D., Baertsch, N.A., Varga, A.G., Baghdodan, H.A., Lydic, R., Morris, K.F., Bolser, D.C., Levitt, E.S., 2021. Neuronal mechanisms underlying opioid-induced respiratory depression: our current understanding. *J. Neurophysiol.* 125 (5), 1899–1919.

- Robert, M., Jouanjus, E., Khouri, C., Fouill   Sam-La  , N., Revol, B., 2023. The opioid epidemic: a worldwide exploratory study using the WHO pharmacovigilance database. *Addiction* 118 (4), 771–775.
- Robinson, A., Wermeling, D.P., 2014. Intranasal naloxone administration for treatment of opioid overdose. *Am. J. Health Syst. Pharm.* 71 (24), 2129–2135.
- Rosal, N.R., Thelmo Jr., F.L., Tzarnas, S., DiCalvo, L., Tariq, S., Grossman, C., 2021. Wooden chest syndrome: a case report of fentanyl-induced chest wall rigidity. *J. Invest. Med. High Impact Case Rep.* 9, 23247096211034036.
- Sobanski, P., Krajnik, M., Shaqura, M., Bloch-Boguslawska, E., Sch  fer, M., Mousa SA., 2014. The presence of mu-, delta-, and kappa-opioid receptors in human heart tissue. *Heart Vessels* 29 (6), 855–863.
- Sporkert, F., Pragst, F., 2000. Determination of methadone and its metabolites EDDP and EMDP in human hair by headspace solid-phase microextraction and gas chromatography–mass spectrometry. *J. Chromatography b: Biomed. Sci. Applic.* 746 (2), 255–264.
- Stancescu, M., Molnar, P., McAleer, C.W., McLamb, W., Long, C.J., Oleaga, C., Prot, J.M., Hickman, J.J., 2015. A phenotypic in vitro model for the main determinants of human whole heart function. *Biomaterials* 60, 20–30.
- Sung, J.H., Kam, C., Shuler, M.L., 2010. A microfluidic device for a pharmacokinetic–pharmacodynamic (PK–PD) model on a chip. *Lab Chip* 10 (4), 446–455.
- van Lunteren, E., Moyer, M., 2012. The effects of K(+) channel blockade on eccentric and isotonic twitch and fatiguing contractions in situ. *Front. Physiol.* 3, 383.
- van Lunteren, E., Pollarine, J., 2010. Improvement of diaphragm and limb muscle isotonic contractile performance by K+ channel blockade. *J. Neuroeng. Rehabilitation* 7 (1), 1.
- Wang, X., Hayes, J.A., Revill, A.L., Song, H., Kottick, A., Vann, N.C., LaMar, M.D., Picardo, M.C., Akins, V.T., Funk, G.D., Del Negro, C.A., 2014. Laser ablation of Dbx1 neurons in the pre-B  tzinger complex stops inspiratory rhythm and impairs output in neonatal mice. *Elife* 3, e03427.
- Wilkinson, G.R., 1996. Cytochrome P4503A (CYP3A) metabolism: prediction of in vivo activity in humans. *J. Pharmacokinet. Biopharm.* 24 (5), 475–490.
- Wu, R., Li, J.-X., 2020. Toll-like receptor 4 signaling and drug addiction. *Front. Pharmacol.* 11.
- Zare, N., Pourhadi, M., Vaseghi, G., Haghjooy Javanmard, S., 2023. The potential interplay between opioid and the toll-like receptor 4 (TLR-4). *Immunopharmacol. Immunotoxicol.* 45 (2), 240–252.